

# Action-Agnostic Point-Level Supervision for Temporal Action Detection

Shuhei M. Yoshida<sup>1</sup>, Takashi Shibata<sup>1</sup>, Makoto Terao<sup>1</sup>, Takayuki Okatani<sup>2,3</sup>, and Masashi Sugiyama<sup>3,4</sup>

<sup>1</sup>Visual Intelligence Research Laboratories, NEC Corporation, Kanagawa 211-8666, Japan

<sup>2</sup>Graduate School of Information Sciences, Tohoku University, Miyagi 980-8579, Japan

<sup>3</sup>RIKEN Center for Advanced Intelligence Project, Tokyo 103-0027, Japan

<sup>4</sup>Graduate School of Frontier Sciences, The University of Tokyo, Chiba 277-8561, Japan

## Abstract

We propose action-agnostic point-level (AAPL) supervision for temporal action detection to achieve accurate action instance detection with a lightly annotated dataset. In the proposed scheme, a small portion of video frames is sampled in an unsupervised manner and presented to human annotators, who then label the frames with action categories. Unlike point-level supervision, which requires annotators to search for every action instance in an untrimmed video, frames to annotate are selected without human intervention in AAPL supervision. We also propose a detection model and learning method to effectively utilize the AAPL labels. Extensive experiments on the variety of datasets (THUMOS '14, FineAction, GTEA, BEOID, and ActivityNet 1.3) demonstrate that the proposed approach is competitive with or outperforms prior methods for video-level and point-level supervision in terms of the trade-off between the annotation cost and detection performance.<sup>1</sup>

## 1 Introduction

Temporal action detection is a vital research area in computer vision and machine learning, primarily focusing on recognizing and localizing human actions and events in untrimmed video sequences [48, 44]. With the rapid growth of video data available online, developing algorithms capable of understanding and interpreting such a wealth of information is critical for a wide range of applications, including anomalous event detection in surveillance videos [45, 41] and sports activity analysis [12, 6]. The existing literature generally tackles action detection problems through fully supervised approaches [26, 49, 50], which require training data with complete action labels and their precise temporal boundaries. Despite significant progress in recent years, these methods confront considerable challenges due to the high annotation cost to predict actions in complex and diverse video settings accurately. To reduce the annotation cost for temporal action detection, weak supervision, such as video-level supervision [42, 47, 2, 23] and point-level labels [34, 31], has been studied. However, these types of supervision have their own difficulty in practice.

<sup>1</sup>An annotation tool to produce AAPL labels and the experimental code for training and testing are available at <https://github.com/smy-nec/AAPL>.



Figure 1: Illustration of ground-truth (full supervision), point-level supervision, and AAPL supervision. The red boxes and lines represents the frames labeled as “Volleyball Spiking”, and the black lines represents those labeled as “Background”. The images are from a video in THUMOS '14 [16].

Video-level supervision only uses the action classes pre-sent in the video as labels. Various approaches have been proposed, such as multiple instance learning-based [47, 37], feature erasing-based [40], and attention-based [36, 20, 28], but they ultimately reduce action detection learning to video classification. Behind this strategy is the assumption that the discriminative intervals contributing to classification are where the actions occur, which is not always true. In addition, when a video contains multiple action classes, it becomes a multi-label classification problem, which is extremely difficult. These limitations severely limit the range of applications of video-level supervision.

Point-level supervision specifies for each action instance a single arbitrary time point in the instance and the action class and has been actively studied recently [17, 19, 22, 24]. While the point-level labels convey partial information about the location of action instances, they do not tell where the actions are *not*. This is a fundamental difficulty in point-level supervised learning of action detection because localization is to distinguish actions from non-actions. In addition, the requirement that action instances must be exhaustively labeled makes the annotation process expensive.

To achieve better trade-off between the annotation costs and detection accuracy, we propose action-agnostic point-level (AAPL) supervision, a novel form of weak supervision for temporal action detection (Fig. 1). In producing AAPL labels, a small portion of video frames is sampled and presented to human annotators, who label the frames with action categories. Unlike point-level supervision, where annotators need to find all action instances in untrimmed videos, the frames to annotate are selected without human intervention. We also propose a baseline learning protocol exploiting the AAPL labels. Our pro-

	Instance-level localization				Video-level classes
	Available	Foreground	Background	Exhaustive	Exhaustive
Full	✓	Complete	Complete	✓	✓
Video	✗	—	—	—	✓
Point	✓	Single point	✗	✓	✓
AAPL (ours)	✓	Point(s)	Point(s)	✗	✗

Table 1: Comparison of full, video-level, point-level, and AAPL supervision. The first set of columns compares them from the perspective of four aspects of instance-level localization: whether information localizing action instances is available, what type of localization is given for foreground and background, and whether all the action instances are exhaustively annotated. The last column shows whether these types of supervision exhaustively give action classes appearing in each video.

posed method, such as the point loss, the video loss, and the prototype-anchored supervised contrast loss, adapts ideas from previous studies for the current setting to exploit the AAPL labels. To demonstrate the utility of AAPL supervision in various use cases, we empirically evaluate our approach using five datasets with different characteristics, including BEOID [7], GTEA [10], THUMOS ’14 [16], FineAction [30], and ActivityNet 1.3 [13]. The results show that the proposed method is competitive with or outperforms prior methods for video-level and point-level supervision. We visualize the trade-offs between the costs and detection performance and compare AAPL supervision with other supervision types. We also find that even training only with annotated frames can achieve competitive results with the previous studies. This suggests the inherent effectiveness of AAPL supervision.

The contributions of this paper are as follows:

- We propose AAPL supervision, a novel form of weak supervision for temporal action detection, which achieves good trade-offs between the annotation costs and detection accuracy.
- We design an action detection model and loss functions that can leverage the AAPL-labeled datasets.
- Comprehensive experiments on a wide range of action detection benchmarks demonstrate that the proposed approach is competitive with or outperforms previous methods using video-level or point-level supervision in terms of the trade-off between the annotation cost and detection performance.

## 2 Action-Agnostic Point-Level Supervision

We first explain the annotation pipeline for AAPL supervision (Sec. 2.1). Then, we compare AAPL supervision with other forms of weak supervision qualitatively (Sec. 2.2) and in terms of annotation time (Sec. 2.3). Some notations for AAPL labels are also introduced (Sec. 2.4).

### 2.1 Annotation Pipeline

AAPL supervision is characterized by the two-step annotation pipeline consisting of action-agnostic frame sampling and manual annotation. Action-agnostic frame sampling

determines which frames in the training videos to annotate. This can be an arbitrary method that, without any human intervention, selects video frames to annotate. Then, human annotators label the sampled frames with action categories.

Action-agnostic frame sampling is what distinguishes AAPL supervision from conventional point-level supervision. The previous scheme requires that every action instance in a video be annotated with a single time point. This is a challenging task because human annotators need to search videos for every action instance. By contrast, for AAPL supervision, annotators just annotate the sampled frames with action categories, but they do not need to search for action instances.

The simplest examples of action-agnostic frame sampling are regularly spaced sampling and random sampling. The former picks up frames at regular intervals, while the latter selects frames randomly. A strength of these methods is that they are easy to implement, computationally light, and free from any assumption on the videos. As we will see in Sec. 4.4.1, the regular sampling is more preferable than the random one because the latter can result in multiple frames in temporal proximity being selected, leading to redundant annotations. We can also consider more sophisticated sampling strategies that take into account the content of the video. For example, we can use a pre-trained feature extractor to compute the feature representations of the frames and then cluster the frames based on the features. The representative frames of each cluster can be selected for annotation. See Sec. 4.4.1 for performance comparison.

Because sampling at regular intervals is computationally free, it might be suitable as an initial choice. In addition, it involves only one hyper-parameter, the interval length, which can be sensibly determined by using prior knowledge about the dataset, *e.g.*, the duration and frequency of action instances. If one has the computational resources, sophisticated methods like clustering-based sampling can be a good alternative, because it can adapt to the dataset characteristics and potentially provide better performance.

### 2.2 Qualitative Comparison

Here, we contrast AAPL supervision with other types of supervision. Table 1 compares four supervision schemes

	Full	Video	Point	AAPL			
				3 sec.	5 sec.	10 sec.	30 sec.
BEOID	3.72	1.11	2.44	2.09	1.43	0.94	0.45
GTEA	4.49	0.93	3.03	1.98	1.60	1.09	0.53
THUMOS '14	1.92	0.45	1.10	1.31	0.95	0.64	0.36

Table 2: Annotation time relative to the video duration. “Full”, “Video”, and “Point” represent the full segment-level supervision, video-level supervision, and point-level supervision, respectively. “ $T$  sec.” stands for the intervals for AAPL supervision.

for temporal action detection: full, video-level, point-level, and AAPL supervision.

Information about instance-level localization is partially available in the AAPL labels, which do not give the exact starting and ending times of action instances but do include timestamps on them. This is similar to point-level supervision, but AAPL supervision can have multiple labels on a single action instance, conveying more complete information about the action location. It also has labels on background frames, which is crucial for temporal localization because localizing an action entails finding the boundaries between the action and the background. Conventional point-level supervision contains timestamps of foreground frames only, and previous work resorts to a self-training strategy to mine background frames, assuming there is at least one background frame between two point-level labels [19]. This assumption is plausible but has a minor practical meaning for rare actions because in such cases point-level labels are distributed so sparsely that two point-level labels cannot effectively narrow down the location of the action boundaries.

Action-agnostic frame sampling is not guaranteed to find all the action instances in a video, and some action instances might not have labels. This is a potential weakness of AAPL supervision. This is true even at the video level; action-agnostic frame sampling might miss all the instances of an action class that is indeed present in the video. This makes it challenging to apply popular methods such as a video-level loss function, which is known to be effective both for video-level [37] and point-level supervision [31, 19]. However, this problem can be mitigated by a simple modification to the video-level loss introduced in Sec. 3.2.

### 2.3 Measurement of Annotation Time

We measured the annotation time for full, video-level, point-level, and AAPL supervision, using a modified version of the VGG Image Annotator (VIA) [8, 9]. For AAPL supervision, we sampled frames to annotate at regular intervals of 3, 5, 10, and 30 seconds. We had eight workers annotate the videos in BEOID [7], GTEA [10], and THUMOS '14 [16]. The detailed protocol of this measurement is given in Appendix C.

Table 2 shows the measured annotation time relative to the duration of videos, *i.e.*, the minutes it took for one annotator to annotate a 1-minute video. The previous methods (“Full”, “Video”, and “Point”) exhibit the expected ordering that full supervision costs the most, and

that video-level supervision costs the least. On the other hand, the annotation time for AAPL supervision varies with the intervals and is well-approximated by a linear function of the number of labeled frames. This modeling assumes that the annotation time per frame is constant, which is reasonable because the annotation time per frame is dominated by the time to select the action category and is not sensitive to the number of frames to annotate.

The annotation time depends on the dataset’s characteristics, such as the density (*i.e.*, the number per unit length of a video) of action instances and the number of action classes occurring in one video. Indeed, these numbers are much larger in BEOID and GTEA than in THUMOS '14. As a result, annotating videos in BEOID and GTEA takes over twice as long as annotating those in THUMOS '14 for full, video-level, and point-level supervision. By contrast, the variation in the annotation time is relatively small for AAPL supervision because AAPL annotation involves local segments around the frames to label and is insensitive to global characteristics like density. This property makes it easy to apply AAPL supervision in a variety of datasets.

### 2.4 Notations

We introduce notations for AAPL labels. Let  $\mathcal{V}$  be a set of videos. AAPL labels for a video  $V \in \mathcal{V}$  are a set  $\mathcal{L}^V = \{(t_i, \mathbf{y}_i)\}_{i \in [N^V]}$  of pairs of a time stamp  $t_i$  and an action label  $\mathbf{y}_i \in \{0, 1\}^C$ . Here,  $N^V$  is the number of annotated frames,  $C$  is the number of action categories, an action label  $\mathbf{y}_i$  is a 0/1-valued vector with the  $c$ -th component indicating the presence or absence of action of the  $c$ -th class at the time  $t_i$ , and  $[K]$  is the set  $\{1, 2, \dots, K\}$ . An annotated frame might not belong to any action instance. Such a frame is called a background and labeled  $\mathbf{y} = \mathbf{0}$ . Also, if multiple action instances of different categories overlap, the frames in the intersection are annotated with a multi-hot vector representing all the action categories present there.

## 3 AAPL Supervised Learning Method

This section explains our approach to temporal action detection under AAPL supervision. This includes the action detection pipeline predicting action instances from an input video (Sec. 3.1), the training objectives for the prediction model (Sec. 3.2), and the pseudo-labeling strategy to make more effective use of the training data (Sec. 3.3).

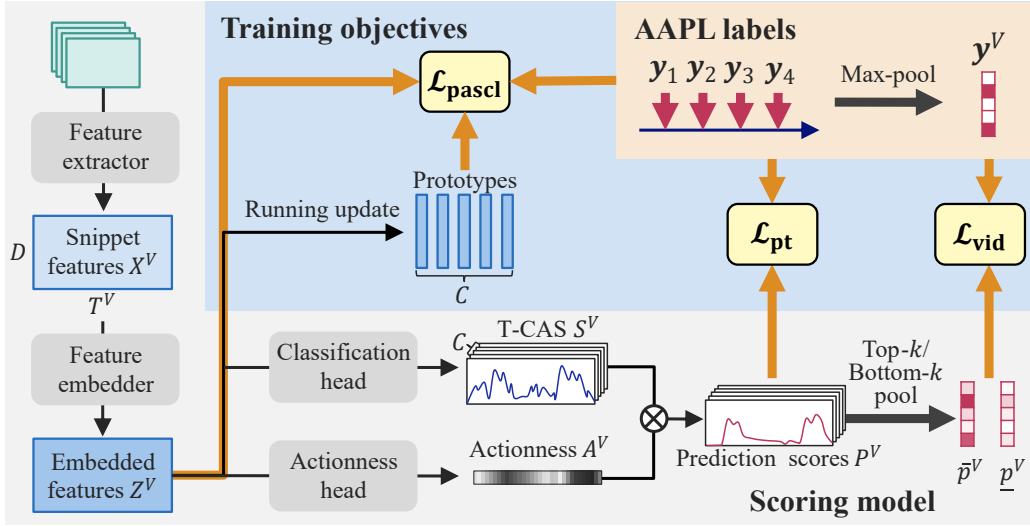


Figure 2: Illustration of the model and the loss functions.

### 3.1 Action Detection Model

Our action detection pipeline consists of preprocessing, snippet scoring, and action instance generation, following previous studies [23]. At the preprocessing stage, we divide an input video into  $T^V$  non-overlapping segments of  $\tau$  frames called snippets and apply the transformation to make them fit the snippet scoring model. The snippet scoring model processes an input video  $V$  into a prediction score sequence  $P^V \in \mathbb{R}^{C \times T^V}$ . The prediction score  $P_{ct}^V$  indicates the likelihood of an action of the  $c$ -th class occurring at time  $t$ . The action instance generator then converts the score sequence into a set of the scored action instances  $\{(s_i, e_i, c_i, p_i)\}_{i \in [M^V]}$  in the video. Here,  $M^V$  is the number of action predictions in the video,  $s_i$  is the starting time,  $e_i$  is the ending time,  $c_i$  is the action category, and  $p_i$  is the confidence score of the  $i$ -th prediction.

The snippet scoring model comprises a feature extractor, a feature embedder, and two scoring heads, as illustrated in Fig. 2. The feature extractor is a pretrained 3D CNN converting each preprocessed snippet into a  $D$ -dimensional snippet feature. We denote the sequence of the snippet features by  $X^V \in \mathbb{R}^{D \times T^V}$ . The feature sequence is further fed into the feature embedder, a temporal convolution layer of the kernel size three followed by the rectified linear unit activation, which outputs the embedded feature sequence  $Z^V = (z_1^V, \dots, z_{T^V}^V) \in \mathbb{R}^{D \times T^V}$ . The embedded features are split into  $Z_S^V \in \mathbb{R}^{D/2 \times T^V}$  and  $Z_A^V \in \mathbb{R}^{D/2 \times T^V}$ , which are then input to the two scoring heads. The classification head classifies each snippet and outputs class-specific classification scores  $S^V \in \mathbb{R}^{C \times T^V}$  called the temporal class activation sequence (T-CAS). The actionness head calculates class-agnostic scores called the actionness sequence  $A^V \in \mathbb{R}^{T^V}$ , which represents the likelihood of a snippet being in an action instance. Both heads combine a point-wise temporal convolution layer and the sigmoid function. We chose the sigmoid instead of the softmax function as the activation for the T-CAS because multiple action instances of different classes might overlap, in which case the model must predict all the

classes present at each moment as positive. The final prediction scores are the product of the two score sequences:  $P_{ct}^V = A_t^V S_{ct}^V$ .

Given the prediction scores for an action category, the action instance generator first upsamples the score sequence to match the frame rate of the input video. It then generates a set of action candidates by collecting the intervals over which the prediction scores are above a threshold  $\theta_{\text{pred}}$ . This process is repeated with several different thresholds. Then, for each action candidate, it calculates the outer-inner contrastive score [39] as the initial confidence score. Finally, soft non-maximum suppression [3] removes duplicate predictions and we calculate the final confidence scores.

### 3.2 Training Objectives for the Scoring Model

Our training objective is the weighted sum of three terms:

$$L = L_{\text{pt}} + \lambda_{\text{vid}} L_{\text{vid}} + \lambda_{\text{pascl}} L_{\text{pascl}}, \quad (1)$$

where  $L_{\text{pt}}$  is the point-level classification loss,  $L_{\text{vid}}$  is the video-level classification loss, and  $L_{\text{pascl}}$  is the prototype-anchored supervised contrastive loss (see Fig. 2). For brevity, we also call them the point loss, the video loss, and the contrastive loss, respectively. Unless otherwise stated, the averaging over a mini-batch of videos is implied in the expressions of the loss functions below.

The **point-level classification loss** quantifies the classification error on labeled snippets. We adopt the focal loss [27] for this purpose. We separate the contributions from the foreground and background snippets,  $L_{\text{pt}} = L_{\text{pt,fg}} + L_{\text{pt,bg}}$ , to handle the class imbalance

between them:

$$L_{\text{pt,fg}} = \frac{-1}{|\mathcal{L}_{\text{fg}}^V|} \sum_{(t,\mathbf{y}) \in \mathcal{L}_{\text{fg}}^V} \left\{ (1 - A_t^V)^2 \log A_t^V + \sum_{c=1}^C [y_c (1 - S_{ct}^V)^2 \log S_{ct}^V + (1 - y_c) (S_{ct}^V)^2 \log(1 - S_{ct}^V)] \right\}, \quad (2)$$

$$L_{\text{pt,bg}} = \frac{-1}{|\mathcal{L}_{\text{bg}}^v|} \sum_{(t,\mathbf{y}) \in \mathcal{L}_{\text{bg}}^v} \left[ (A_t^V)^2 \log(1 - A_t^V) + \sum_{c=1}^c (s_{ct}^v)^2 \log(1 - s_{ct}^v) \right]. \quad (3)$$

Here,  $\mathcal{L}_{\text{fg}}^V = \{(t, \mathbf{y}) \in \mathcal{L}^V \mid \mathbf{y} \neq \mathbf{0}\}$ , and  $\mathcal{L}_{\text{bg}}^V = \{(t, \mathbf{y}) \in \mathcal{L}^V \mid \mathbf{y} = \mathbf{0}\}$ , representing the subsets of AAPL labels on the foreground and background snippets, respectively. Importantly, we can calculate both  $L_{\text{pt,fg}}$  and  $L_{\text{pt,bg}}$  by using human-generated AAPL labels only because AAPL labels have labels on background snippets. By contrast, previous point-level methods [31, 19] require pseudo-labeling to calculate the background point loss. This is a significant advantage of AAPL supervision over previous point-level methods because action localization involves distinguishing foreground actions from the background and having reliable labels on the background snippets is crucial for learning this task.

The **video-level classification loss** measures the agreement between the video-level labels and predictions. This type of loss functions has played a central role in both video-level supervision [47, 37] and It has also been adopted for point-level supervision [31, 19]. These settings have complete video-level labels, *i.e.*, the presence or absence of each action class in each video is known. By contrast, in the AAPL-supervised setting the video-level labels might be incomplete. In other words, the absence of AAPL labels of an action class does not necessarily imply that the class is absent in the video. Consequently, we cannot simply apply the video loss as used in the video-level [47, 37] and point-level [31, 19] scenarios.

To handle this incompleteness, we introduce the positive and negative parts of the video loss. The positive part of the video loss is expressed as

$$L_{\text{vid,pos}} = - \sum_{c \in [C]} y_c^V \log \bar{p}_c^V, \quad (4)$$

where  $\bar{p}_c^V$  is the video-level prediction score,

$$\bar{p}_c^V = \sigma \left( \frac{1}{k_{\text{pos}}} \max_{\mathcal{T} \subset [T^V], |\mathcal{T}|=k_{\text{pos}}} \sum_{t \in \mathcal{T}} \sigma^{-1}(P_{ct}^V) \right), \quad (5)$$

$y_c^V$  is the video-level label,

$$y_c^V = \max_{(t,\mathbf{y}) \in \mathcal{L}^V} y_c, \quad (6)$$

and  $\sigma$  and  $\sigma^{-1}$  represent the sigmoid function and its inverse function. The terms of the form  $(1 - y_c^V) \log(1 - \bar{p}_c^V)$

are excluded in our loss because  $y_c^V = 0$  does not necessarily mean that the  $c$ -th class is absent in the video. This exclusion can lead to a biased estimation of the video-level prediction scores. To compensate this bias, we introduce the negative part of the video loss,  $L_{\text{vid,neg}}$ . To this end, we define  $\underline{p}^V$  by the ‘‘bottom- $k$ ’’ pooling:

$$\underline{p}_c^V = \sigma \left( \frac{1}{k_{\text{neg}}} \min_{\mathcal{T} \subset [T^V], |\mathcal{T}|=k_{\text{neg}}} \sum_{t \in \mathcal{T}} \sigma^{-1}(P_{ct}^V) \right). \quad (7)$$

This represents the average scores of frames that are not likely in the  $c$ -th class. Then, the negative part is written as

$$L_{\text{vid,neg}} = - \sum_{c \in [C]} \log(1 - \underline{p}_c^V). \quad (8)$$

The total video loss is the simple sum of the two parts:  $L_{\text{vid}} = L_{\text{vid,pos}} + L_{\text{vid,neg}}$ .

Following recent work [14, 29, 19, 22] demonstrating that enhancing the discriminative power of embedded features improves action detection performance, we also introduce the **prototype-anchored supervised contrastive loss**. This loss was inspired by the SupCon loss [18] and utilizes AAPL labels to enhance the embedded features. The anchors in the SupCon loss are replaced with the prototypes. This modification makes our loss computationally more efficient.

To formulate the prototype-anchored supervised contrastive loss, we first introduce the prototype  $\mathbf{q}_c$  for the  $c$ -th action class. The prototype is the running estimate of the average embedded features for snippets belonging to action instances of the  $c$ -th class. The prototype  $\mathbf{q}_c$  is initialized as

$$\mathbf{q}_c = \frac{1}{|\mathcal{L}_c|} \sum_{(V,t,\mathbf{y}) \in \mathcal{L}_c} \mathbf{z}_t^V, \quad (9)$$

where  $\mathcal{L}_c = \{(V, t, \mathbf{y}) \mid \forall V \in \mathcal{V}, (t, \mathbf{y}) \in \mathcal{L}^V, y_c = 1\}$  is the set of all the AAPL labels attached to  $c$ -th class action snippets in the training dataset. During the training,  $\mathbf{q}_c$  is updated at every iteration as

$$\mathbf{q}_c \leftarrow (1 - \mu) \mathbf{q}_c + \frac{\mu}{|\mathcal{L}_c^{\mathcal{B}}|} \sum_{(V,t,\mathbf{y}) \in \mathcal{L}_c^{\mathcal{B}}} \mathbf{z}_t^V, \quad (10)$$

where  $\mathcal{L}_c^{\mathcal{B}}$  is a subset of  $\mathcal{L}_c$  from the videos in the mini-batch for that iteration.

Using the prototypes, the prototype-anchored supervised contrastive loss for a mini-batch  $\mathcal{B}$  is expressed as

$$L_{\text{pascl}} = \sum_{c \in [C]} \frac{-1}{|\mathcal{L}_c^{\mathcal{B}}|} \times \sum_{(V,t,\mathbf{y}) \in \mathcal{L}_c^{\mathcal{B}}} \log \left[ \frac{e^{\mathbf{q}_c \cdot \mathbf{z}_t^V / \tau}}{\sum_{(V',t',\mathbf{y}') \in \mathcal{L}_c^{\mathcal{B}}} e^{\mathbf{q}_c \cdot \mathbf{z}_{t'}^{V'} / \tau}} \right], \quad (11)$$

where  $\mathcal{L}^{\mathcal{B}} = \cup_{c \in [C]} \mathcal{L}_c^{\mathcal{B}}$ . Because  $L_{\text{pascl}}$  is calculated using all the videos in the mini-batch, we do not apply mini-batch averaging to  $L_{\text{pascl}}$ . This loss function pulls the embedded features of the  $c$ -th action class to  $\mathbf{q}_c$  while repelling the others from it. We do not use a prototype for background features, and therefore, such features are repelled by all the prototype vectors.

Supervision	Method	mAP@IoU [%] (BEOID)					mAP@IoU [%] (GTEA)				
		0.1	0.3	0.5	0.7	Avg	0.1	0.3	0.5	0.7	Avg
Point	Ma et al. [31]	62.9	40.9	16.7	3.5	30.9	58.0	37.9	19.3	11.9	31.0
	Ju et al. [17]	63.2	46.8	20.9	5.8	34.9	59.7	48.3	21.9	18.1	33.7
	Li et al. [24]	71.5	40.3	20.3	5.5	34.4	60.2	44.7	28.8	12.2	36.4
	Lee and Byun [19]	76.9	61.4	42.7	25.1	51.8	63.9	55.7	33.9	20.8	43.5
	Li et al. [22]	<b>78.7</b>	63.3	44.1	<b>26.9</b>	53.3	65.2	<b>56.8</b>	34.3	21.2	44.9
AAPL (3 sec.)	<i>Ours</i>	75.5	<b>67.6</b>	<b>48.5</b>	26.3	<b>55.2</b>	<b>70.3</b>	54.4	<b>37.7</b>	<b>23.4</b>	<b>46.3</b>

Table 3: Detection performance on GTEA and BEOID. Each column shows the mAP at a specific IoU threshold (0.1, 0.3, 0.5, and 0.7) and the average mAP (Avg) over the thresholds.

### 3.3 Ground-Truth Anchored Pseudo-Labeling

Among the loss functions in the previous section, the point loss  $L_{pt}$  and the contrastive loss  $L_{pascl}$  do not involve unlabeled snippets, which constitute the majority of the snippets in the training dataset. Pseudo-labeling offers a convenient way of exploiting these underutilized data by generating pseudo labels from the predictions and using them in calculating the losses. To obtain a better outcome, the quality of the pseudo labels is crucial.

Here, we adopt the ground-truth anchored pseudo-labeling strategy, inspired by Ma et al. [31] and Li et al. [22]. Under this strategy, pseudo-labels of the  $c$ -th action class are assigned to the snippets on an interval if (i) the prediction scores  $P_c^V$  over the interval are above a threshold  $\theta_{fg}$ , (ii) at least one of the snippets is annotated with an AAPL label, and (iii) every AAPL label  $(t, \mathbf{y})$  on the interval satisfies  $y_c = 1$ . Put differently, pseudo-labels are given to intervals with highly confident predictions consistent with AAPL labels. Similarly, pseudo-background labels are assigned to an interval if (a) the actionness scores are below a threshold  $\theta_{bg}$  over the interval, and (b) there is at least one background label and no foreground action label on the interval. When calculating the point loss and the contrastive loss, we replace the AAPL labels with the pseudo labels.

## 4 Experiments

In this section, we empirically evaluate the effectiveness of AAPL supervision for temporal action detection. As action-agnostic frame sampling, we use the regularly spaced sampling, except in the part of Sec. 4.4.1 that compares different sampling schemes. We also analyze the effects of our design choices. We defer details of implementation and hyper-parameters to Appendix B.

### 4.1 Datasets

To demonstrate the usefulness in various usecases, we use five benchmark datasets with different characteristics. Here, we provide a brief overview of the datasets. More dataset statistics are shown in Appendix A.

**BEOID** [7] is a dataset of egocentric activity videos, containing diverse activities ranging from cooking to work-outs. We adopt the training-validation split from Ma et al. [31].

**GTEA** [10] also consists egocentric videos but focuses fine-grained daily activities in a kitchen. The median number of action instances per video is 18 in an about 60-second video. This number is by far the largest among the datasets used in this paper.

**THUMOS '14** [16] has significant variations in the lengths and the number of occurrences of action instances. Following the convention [47, 36], we use the validation set for training and the test set for evaluation.

**FineAction** [30] is a large scale dataset for fine-grained action detection. The fine-grained nature of action categories and the sparsity of action instances make this dataset extremely challenging for action detection.

**ActivityNet 1.3** [13] is a large-scale video dataset for action recognition and detection of 200 diverse action categories. The majority of videos in this dataset have only one action instance, and the duration of each action instance is much longer than that of the other datasets.

### 4.2 Evaluation Metrics

As evaluation metrics, we report mean average precision (mAP) at various thresholds for temporal intersection over union (IoU) (see Jiang et al. [16] for the formal definition). Following convention [19, 25], when calculating the average mAP (Avg mAP), we average mAP's at the thresholds from 0.1 to 0.7 with a step 0.1 for BEOID, GTEA, and THUMOS '14, and from 0.5 to 0.95 with a step 0.05 for FineAction and ActivityNet 1.3. All the reported results of our method are the average of eight runs with different random seeds.

### 4.3 Main Results

Table 3 provides the experimental results on BEOID and GTEA, demonstrating that our method outperforms the point-level methods in terms of the average mAP. The intervals of the AAPL labels are three seconds, which incurs less annotation costs than that for the point-level labels, as shown in Sec. 2.3. Therefore, the results in Tab. 3 not just show the better accuracy of the proposed method but also indicate the superiority of our approach regarding the trade-off between detection performance and annotation time.

Figure 3 shows the trade-off between detection performance and annotation time for AAPL-supervised learning

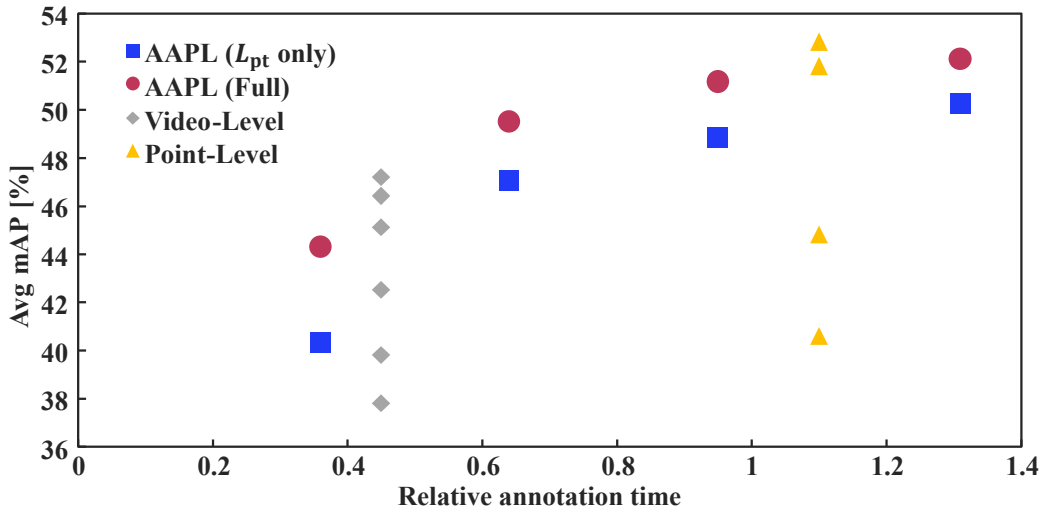


Figure 3: Trade-off between detection performance and annotation time. The blue squares represent AAPL-supervised training with  $L_{pt}$  only, the red circles represent that with our full objective, the gray diamonds represent video-level methods [37, 33, 38, 15, 5, 46], and the yellow triangles represent point-level methods [31, 17, 19, 22].

Supervision	Method	mAP@IoU [%]			
		0.50	0.75	0.95	Avg
Video	Paul et al. [37] <sup>†</sup>	6.2	3.2	0.8	3.5
	Lee et al. [21] <sup>†</sup>	6.7	3.2	1.0	3.6
	Ma et al. [32] <sup>†</sup>	6.8	2.7	0.8	3.3
	Narayan et al. [35] <sup>†</sup>	6.8	3.0	0.8	3.4
	Li et al. [25]	7.1	4.0	1.1	4.1
Point	Lee and Byun [19] <sup>‡</sup>	7.8	3.2	0.1	3.5
AAPL (30 sec.)	<i>Ours</i>	10.6	5.4	1.8	6.0

Table 4: Comparison of detection performance on FineAction. <sup>†</sup> indicates the results reproduced by [25], and <sup>‡</sup> indicates those reproduced by us (see Appendix B.3 for details).

on THUMOS ’14, including the results with our full objective and with  $L_{pt}$  only. The intervals between AAPL labels are 3, 5, 10, and 30 seconds, which are converted to the annotation times using Tab. 2. For comparison, it also shows the results of previous one-stage training methods for video-level [37, 33, 38, 15, 5, 46] and point-level [31, 17, 19, 22] supervision. For a fixed budget of annotation time, our full objective for AAPL supervision is competitive with the state-of-the-art methods for the other types of supervision. In addition, our baseline using  $L_{pt}$  only already outperforms many of the previous methods. Even the baseline with 30-second-interval AAPL labels achieves the average mAP comparable to that of Ma et al. [31], even though such sparse AAPL labels can be produced in one-third of the annotation time for point-level labels. This strength of the simple baseline illustrates the inherent effectiveness of AAPL supervision.

The results on FineAction are shown in Table 4. It shows that even our proposed method with the most sparse labels outperforms all the previous methods, demonstrating the strength of AAPL supervision with fine-grained and sparse actions. Interestingly, LACP by Lee and Byun [19], the point-level method outperforming all the video-level methods on THUMOS ’14, struggles with FineAc-

tion and falls short of the point-level approach, HAAN by Li et al. [25]. We conjecture this is because of the sparsity of action instances in FineAction videos. Very sparse point-level labels can enable the model to locate likely frames in actions but might not be informative enough to help a detection model localize action boundaries. This hypothesis is consistent with the fact that LACP outperforms HAAN in terms of mAP@0.5, while lagging behind the latter at larger IoU thresholds; LACP successfully found the actions but failed to localize them.

Table 5 shows the results on ActivityNet 1.3. For all the intervals we experimented with, our method achieved the detection accuracy comparable or superior to Lee and Byun [19], the state-of-the-art point-level method.

#### 4.4 Analysis

In this section, we analyze and justify some of the design choices in our approach.

##### 4.4.1 Action-Agnostic Frame Sampling.

The design of action-agnostic frame sampling impacts the detection performance. To illustrate this, we conducted experiments with three different sampling schemes:



Supervision	Method	mAP@IoU [%]			
		0.5	0.75	0.95	Avg
Point	Lee and Byun [19]	40.4	24.6	5.7	25.1
AAPL (10 sec.)	<i>Ours</i>	41.3	25.4	5.8	25.7
AAPL (30 sec.)	<i>Ours</i>	39.6	24.3	5.6	24.7

Table 5: Detection performance on ActivityNet 1.3

	THUMOS '14				BEOID
	3 sec.	5 sec.	10 sec.	30 sec.	3 sec.
Random sampling	49.9	49.9	48.2	43.8	44.7
Regular intervals	52.1	51.2	49.5	44.3	<b>55.2</b>
Clustering	<b>52.9</b>	<b>51.6</b>	<b>50.2</b>	<b>45.7</b>	51.6

Table 6: Comparison of different methods of action-agnostic frame sampling in terms of Avg mAP [%]. The second row shows the average interval between AAPL labels.

$L_{pt}$	$L_{vid}$	$L_{pascl}$	PL	Avg mAP [%]	
				THUMOS '14	BEOID
✓				40.3	32.0
✓	✓			42.8	46.2
✓	✓	✓		43.6	54.1
✓	✓	✓	✓	<b>44.3</b>	<b>55.2</b>

Table 7: Effectiveness of each component. AAPL labels for THUMOS '14 are sampled at intervals of 30 seconds, and those for BEOID are sampled at intervals of 3 seconds. "PL" stands for ground-truth anchored pseudo-labeling.

random sampling, regular intervals, and clustering-based sampling. The clustering-based sampling first performs  $k$ -means clustering on snippet features extracted using a pre-trained model and then selects the frames closest to the cluster centers (see Appendix B.4 for details). As shown in Tab. 6, the sampling at regular intervals and the clustering-based sampling consistently outperform random sampling.

This suggests that annotating diverse frames is crucial for achieving good detection performance. Indeed, both the regular-interval sampling and the clustering-based sampling tend to enhance the diversity of the annotated frames: the former does so by reducing the temporal correlation between the annotated frames, and the latter by selecting frames that are separated in the embedding space. Which of the two is better depends on the dataset, as shown in Tab. 6.

#### 4.4.2 Effectiveness of Each Component.

The proposed loss function consists of three components:  $L_{pt}$ ,  $L_{vid}$ , and  $L_{pascl}$ . We also adopt the ground-truth anchored pseudo-labeling (PL) strategy. To evaluate the effectiveness of each component, we conducted the ablation study, as shown in Tab. 7. For both THUMOS '14 and BEOID, adding each component improves the detection accuracy, and the full objective achieves the best

performance. The video loss makes particularly large contributions, showing that the self-training strategy based on top-/bottom- $k$  pooling is effective with AAPL supervision, as with conventional weak supervision.

#### 4.4.3 Form of the Video Loss.

The proposed video loss is adapted specifically for AAPL supervision to handle the incompleteness of the video-level labels. To demonstrate the effectiveness of our design of the video loss, we compare our proposed video loss with the binary cross-entropy (BCE loss), which is the de facto standard in the field [19, 22]. As shown in Tab. 8, the forms of the video loss impact the detection performance. In particular, mAP's at lower IoU thresholds are affected more than those at higher thresholds. This is reasonable because the video loss, as a ranking-based pseudo-labeling strategy, does not concern the accurate localization of action instances but does help mine unlabeled instances.

## 5 Conclusion

We proposed action-agnostic point-level (AAPL) supervision for temporal action detection to achieve a better trade-off between action detection performance and annotation costs. We also proposed an action detection model and the training method to exploit AAPL-labeled data. Extensive empirical investigation suggested that AAPL supervision was competitive with or outperformed previous supervision schemes for a wide range of action detection benchmarks in terms of the cost-performance trade-off. Further analyses justified our design choices, such as frame sampling at regular intervals and the form of the video loss.

## Acknowledgments

We thank Ryoma Ouchi for his efforts and commitment at the early stage of this project.



	mAP@IoU [%] (THUMOS '14)					mAP@IoU [%] (BEOID)				
	0.1	0.3	0.5	0.7	Avg	0.1	0.3	0.5	0.7	Avg
$L_{\text{pt}}$ only	60.1	51.4	33.6	13.3	40.3	45.3	38.4	29.2	12.3	32.0
$L_{\text{pt}} + \text{BCE loss}$	61.4	52.1	34.0	12.6	40.8	56.8	50.6	38.1	<b>19.2</b>	42.0
$L_{\text{pt}} + L_{\text{vid}}$ (Ours)	<b>64.3</b>	<b>54.6</b>	<b>35.2</b>	<b>14.0</b>	<b>42.8</b>	<b>64.0</b>	<b>56.1</b>	<b>42.0</b>	18.2	<b>46.2</b>

Table 8: Comparison of video losses. AAPL labels for THUMOS '14 are sampled at intervals of 30 seconds, and those for BEOID are sampled at intervals of 3 seconds.

Dataset name	Classes	Number of videos		Duration [sec]		Number per video	
		Training	Validation	Video	Action	Actions	Classes
BEOID [7]	34	46	12	45.3	1.2	6	3
GTEA [10]	7	21	7	62.8	1.8	18	6
THUMOS '14 [16]	20	200	213	150.4	2.9	8	1
FineAction [30]	106	8,440	4,174	101.5	1.3	2	1
ActivityNet 1.3 [13]	200	10,024	4,926	114.3	26.8	1	1

Table 9: Basic dataset statistics. Here, the column ‘‘Classes’’ shows the number of action categories, ‘‘Number of videos’’ shows the number of videos in the training and validation sets, ‘‘Duration’’ shows the median duration of the training videos and action instances, and ‘‘Number per video’’ shows the median numbers of action instances and unique action classes in one training video.

## Appendix

### A Dataset Statistics

In Tab. 9 we provide the basic statistics of the datasets [7, 10, 16, 30, 13] used in the experiments to facilitate readers’ qualitative understanding of the experiments and measurement.

Most videos in BEOID and GTEA contain action instances of multiple classes, while those in the other datasets typically have instances of only one class. They also have many action instances in one minute of a video. Because of these differences, the two datasets are highly challenging for the video-level setting. Indeed, despite their popularity in the literature on point-level supervision, they have not been used to benchmark weakly supervised temporal action localization using video-level labels.

THUMOS '14 and ActivityNet 1.3 frequently appear in the action detection literature. A video in THUMOS '14 typically has action instances of only one class, but the number of action instances is also prominent in some videos. The dataset has significant variation in the duration and the number of action instances, which makes this a challenging benchmark. By contrast, most videos in ActivityNet 1.3 have only one action instance, and each action instance has a long duration compared with the other datasets. ActivityNet 1.3 stands out in terms of scale, with the number of videos being significantly larger than BEOID, GTEA, and THUMOS '14. This large-scale dataset provides a diverse range of action classes.

The FineAction dataset is the newest of the five datasets. Its scale is comparable to ActivityNet 1.3, but the fine-grained nature of action classes and the relatively short duration and the sparsity action instances make it challenging even for point-level supervision, which has achieved

superior performance on THUMOS '14 and ActivityNet 1.3 compared with video-level supervision.

### B Details on Experiments

In this section, we provide the details of the experiments that are omitted in the main text.

#### B.1 Implementation Details

In this section, we explain the details of the implementation of our method.

##### B.1.1 Snippet Features.

As the feature extractor, we employed the two-stream Inflated-3D (I3D) Inception-V1 model trained on Kinetics-400 [4]. It takes 16 frames of RGB and optical flow, *i.e.*,  $N_S = 16$ , and outputs 1024-dimensional feature vectors for each input modality. The snippet features were extracted before the experiments were conducted, *i.e.*, the feature extractor was frozen, and only the embedder and two heads were updated during training. The two-stream features are concatenated into a single snippet feature of 2048 dimensions, except for FineAction [30], whose two-stream feature has 4096 dimensions. For GTEA and BEOID, we used I3D features extracted and distributed by [31]. For FineAction, we used I3D features made public by the original dataset provider [30]. Following the previous work [25], we adopted the ‘‘I3D\_100’’ features, which the dataset provider generated by temporally scaling the snippet feature sequence to the fixed length of 100 by linear interpolation.

The FineAction paper [30] asserts that they have extracted snippet features using ‘‘I3D model’’ with citation

of the I3D paper [4]. The latter paper implemented the model as the 3D version of Inception-V1 [43], which outputs 2048-dimensional features in the two-stream setting. However, the distributed features of FineAction have 4096 dimensions. As of writing this paper, we have not figured out the exact setting in which the features were extracted, but we used the distributed features as they were for a fair comparison with previous work using the same features [25].

The videos in a training dataset have varying durations, which result in varying lengths of snippet feature sequences. To facilitate mini-batch training, we sampled the snippet feature sequences to a fixed length. The sampled sequence lengths are 750 for THUMOS ’14, 50 for ActivityNet 1.3, and 100 for the other datasets.

### B.1.2 Scoring Model.

As the feature embedder, we employed a single convolution layer with kernel size three, followed by the ReLU activation function. The input and output of the embedder are the same shape.

The classification and actionness heads accept half of the embedded features, *e.g.*, in the case of THUMOS ’14 (or any dataset other than FineAction), the first 1024 dimensions of the embedded features are fed into the classification head, while the others are consumed by the actionness head. Then, the heads apply the point-wise convolution and the sigmoid activation function. During the training, the dropout is also applied before the point-wise convolution. The dropout rate is set at 0.7 for all the experiments.

### B.1.3 Parametrization of the Top- $k$ Pooling.

Following previous work [37, 20, 38], we set  $k_X$  in the top- $k$  pooling as  $k_X = \min\{1, \lfloor T/r_X \rfloor\}$ , where  $X$  is either fg or bg,  $T$  is the length of the snippet feature sequence, and  $r_X$  is a hyper-parameter. We borrowed the values of  $r_{fg}$  and  $r_{bg}$  from the previous work [38] and set  $(r_{fg}, r_{bg})$  as  $(8, 3)$  for the datasets other than ActivityNet 1.3 and  $(2, 10)$  for ActivityNet 1.3.

### B.1.4 Optimization.

The scoring model was optimized using the Adam optimizer with batch size 16. The learning rate and weight decay were tuned by grid search.

## B.2 Hyper-Parameters

The hyper-parameters of the scoring model were tuned using the grid search. Because optimizing many hyper-parameters is computationally expensive, we incrementally tuned the hyper-parameters. Specifically, we first tuned the learning rate and weight decay, then the weight of the video loss  $\lambda_{vid}$ , then the weight of the contrastive loss  $\lambda_{pascl}$  and the temperature  $\tau$ , and finally the thresholds  $\theta_{fg}$  and  $\theta_{bg}$  for the ground-truth anchored pseudo-labeling. From preliminary experiments, we found that the momentum parameter  $\mu$  of the prototype update for the contrastive loss, and therefore, we fixed it to 0.001 for

all the experiments. The optimal values are summarized in Appendix B.2.

## B.3 LACP Experiment on FineAction

The evaluation of LACP [19] on FineAction was conducted using the code developed by LACP’s authors<sup>2</sup>. We modified the code to adapt it to the FineAction dataset and its evaluation metric.

Under the default configuration for THUMOS ’14, the optimal sequence search (OSS) [19] runs once in every ten iterations, but with the dataset as large as FineAction, this frequency makes the training extremely inefficient. Therefore, we dropped the frequency of OSS to once in every 200 iterations, which was 20 times as infrequent as the default value. However, this is twice as frequent in terms of epochs as the default. We also swept the interval of 100 to 500 iterations and verified that the 200-iteration interval achieved the peak detection accuracy.

Other hyper-parameters were tuned using the grid search. The optimal values that are different from the default are the learning rate  $2 \times 10^{-5}$  and  $r_{act} = 2$ .

## B.4 Clustering-Based Frame Sampling

Here, we describe the specific implementation of action-agnostic frame sampling based on clustering. The pseudo-code is presented in Algorithm 1. Basically, we perform the  $k$ -means clustering on the set of snippet features extracted by using pretrained feature extractor. This algorithm is grounded on the assumption that it is more desirable to sample diverse frames.

We adopted the same feature extractor as the detection model, *i.e.*, the Inflated 3D (I3D) convolutional neural network [4] trained on the Kinetics dataset. Feature vectors output by the I3D model have 2048 dimensions, but such high-dimensional features are not suitable for clustering. For this reason, we apply the principal component analysis to reduce the dimensions to 64. The number of clusters for a video is set to be  $T^V/\tau$ , where  $T^V$  is the duration of the video  $V$ , and  $\tau$  is the average interval of labeled frames.

## C Measurement of Annotation Time

To demonstrate that the sparse supervision has benefits for annotation costs, we measured actual annotation speed for three datasets, THUMOS ’14 [16], GTEA [10], and BEIOD [7]. This section explains the detailed protocol of the measurement.

### C.1 Randomized Allocation

The annotation time depends not only on the annotation method and the dataset but also on various factors, such as an annotator’s proficiency in the annotation method and familiarity with the dataset. There can also be an issue of compatibility between videos and annotation methods;

<sup>2</sup><https://github.com/Pilhyeon/Learning-Action-Completeness-from-Points/tree/1ef066a4d754b5a8c6993de5afc20898eea46118>

Dataset	LR	WD	$\lambda_{\text{vid}}$	$\lambda_{\text{pascl}}$	$\tau$	$\theta_{\text{fg}}$	$\theta_{\text{bg}}$
THUMOS '14	0.0001	0.001	3.0	0.1	0.10	1.0	0.05
FineAction	0.0001	0.0001	0.003	0.01	0.1	1.0	0.5
GTEA	0.0001	0	0.3	0.03	0.3	0.5	0.0
BEOID	0.001	0.0001	0.3	30.0	0.3	0.5	0.0
ActivityNet 1.3	0.0001	0.0001	0.001	0.001	1	0.95	0.5

Table 10: Optimal hyper-parameters for the scoring model. “LR” and “WD” are the abbreviations of the learning rate and weight decay, respectively. The vertical lines group the hyper-parameters that were tuned together.

---

### Algorithm 1 Clustering-based frame sampling

---

**Require:**  $V$ : Video,  $k$ : The number of frames to sample,  $M$ : Pre-trained feature extractor,  $D$ : The number of principle components.

**Ensure:** List of frames to pass to human annotators

- 1: Divide  $V$  into a list of snippets  $\mathcal{S}$ .
  - 2: Let  $\mathcal{Z}$  be an empty list.
  - 3: **for all**  $S \in \mathcal{S}$  **do**
  - 4:   Append  $M(S)$  to  $\mathcal{Z}$ .
  - 5: **end for**
  - 6: Apply PCA on  $\mathcal{Z}$  to get  $\mathcal{Z}_{\text{PCA}}$  with  $D$  dimensions.
  - 7: Apply  $k$ -means on  $\mathcal{Z}_{\text{PCA}}$ .
  - 8: Collect the cluster closest to the center of each cluster.
  
  - 9: **return** the center frames from the collected snippets.
- 

some videos might be easier to annotate by one method than others, and vice versa by another method. Ideally, it would be desirable to measure the annotation time for the same set of videos using different annotation methods while equalizing the effects of these factors. However, such an ideal measurement is impossible because annotators become familiar with the annotation method and the dataset as they proceed with the annotation. To overcome this problem, we employed the randomized allocation strategy.

To this end, we hired eight workers and randomly allocated videos and annotation methods. First, we arranged the videos in each dataset in a random order. Next, we randomly assigned an annotation method (full, video-level, point-level, or AAPL with different intervals) to each worker for each video. This allocation was carried out using the block randomization strategy [11, 1], which ensures that each annotation method is assigned to each worker for the almost same number of times. By this allocation, we aimed to extract the difference in annotation time that is attributable to the annotation method while mitigating the effects of the annotator’s proficiency in the annotation methods, familiarity with the dataset, and the compatibility issue between videos and the annotation methods.

Note that we reserved a few videos for the training of the workers. These videos were selected so that at least one action instance per class appears in the videos. They were used to familiarize the workers with the annotation methods and the action classes. The reserved videos were not included in the measurement of the annotation time.

## C.2 Annotation Tool

We developed a browser-based annotation tool for the four annotation methods. This tool is the adaptation from VGG Image Annotator [9], an open-source image annotation tool equipped with the functionality for full supervision of temporal action detection. The tool and the manual are available at <https://github.com/smy-nec/AAPL>.

## C.3 Instructions to Annotators

In this section, we provide the instructions given to the annotators, except for the usage of the tool, which is explained in the tool’s manual.

We instructed the workers to start the timer when they were ready to start annotating a video, *i.e.*, when they had finished reading the instructions, loading a VIA project file and a video, and configuring the tool for annotation. We also instructed them to stop the timer when they had reached the end of the video and finished the annotation. After that, the workers were asked to save the project file containing the annotations and the time measurement and to submit the project file to us. In addition, we asked the workers to self-check the annotations. Self-checking for a video was performed immediately after the annotation of the video was finished. The time of the self-checking was measured separately from the first annotation.

Some workers might be so meticulous that they pause and repeat the video to ensure that they produce as accurate annotations as possible. Although we acknowledge the importance of keeping the annotations accurate, this kind of meticulousness can lead to an overestimation of the annotation time. To mitigate this issue, we instruct the workers not to rewind the video unless they need to do so because either

- they have skipped a part of the video (*e.g.*, for AAPL annotation) and need to go back a few seconds to decide the action occurring at that point, or
- they have passed an action boundary and need to go back to mark it,

and even if they did so, we asked them to rewind the video by a few seconds at most.

Regarding self-checking, we only asked them to check and correct clear mistakes such as missing action instances and wrong action classes. We asked not to adjust the action boundaries here because the self-checking is not intended

	Full	Video	Point	3 sec	5 sec	10 sec	30 sec
THUMOS '14	2.994	0.810	1.863	2.272	1.648	1.072	0.644
GTEA	6.105	1.591	4.594	3.138	2.481	1.690	0.855
BEOID	5.205	1.976	3.873	3.305	2.312	1.483	0.827

Table 11: Comparison of the relative annotation time, including the self-checking. Each cell shows the minutes it took for one annotator to annotate a 1-minute video. For AAPL supervision, we sampled frames to annotate at regular intervals of 3, 5, 10, and 30 seconds.

to be a full re-annotation but a quick check for quality control.

The workers were also given the textual definitions of each annotation method with schematic figures like Fig. 1 in the main text. We also provided them with the list of action classes, their definition, and examples of full annotations for the videos reserved for the training of the workers.

#### C.4 On the Measurement Result

The relative annotation time reported in the main text is the total annotation time divided by the total annotated video duration. The time measurement there does not include the time for the self-checking. To complement those data, Tab. 11 shows the relative annotation time that also accounts for the self-checking. This indicates that the comparison of annotation time among different annotation methods is not significantly affected by taking the self-checking into account.

#### C.5 Limitation of the Current Measurement

Actual annotation costs depend not only on the type of supervision but also on many details of an annotation pipeline, including the user interface of annotation software and instructions given to the workers. Also, if the number of action categories is large as in ActivityNet and FineAction, searching a long list for the class of each action instance is unrealistic, and the design of the annotation pipeline must be fundamentally different from the one we implemented in this paper, as in [13]. We would like to emphasize, however, that addressing the trade-offs between detection performance and annotation time is crucial in researching weak supervision schemes, and that measurement like ours is indispensable for this purpose. Therefore, the annotation time as measured in this work should be considered not as the practically realistic value but as a convenient device to compare different supervision schemes on a reasonably equal footing.

## References

- [1] Barak Ariel and David P. Farrington. *Randomized Block Designs*, pages 4273–4283. Springer New York, New York, NY, 2014. ISBN 978-1-4614-5690-2. doi: 10.1007/978-1-4614-5690-2\_52. URL [https://doi.org/10.1007/978-1-4614-5690-2\\_52](https://doi.org/10.1007/978-1-4614-5690-2_52).
- [2] AbdulRahman Baraka and Mohd Halim Mohd Noor. Weakly-supervised temporal action localization: A survey. *Neural Computing and Applications*, 34 (11):8479–8499, June 2022. ISSN 1433-3058. doi: 10.1007/s00521-022-07102-x.
- [3] Navaneeth Bodla, Bharat Singh, Rama Chellappa, and Larry S. Davis. Soft-NMS — Improving Object Detection with One Line of Code. In *2017 IEEE International Conference on Computer Vision (ICCV)*, pages 5562–5570, October 2017. doi: 10.1109/ICCV.2017.593.
- [4] João Carreira and Andrew Zisserman. Quo Vadis, Action Recognition? A New Model and the Kinetics Dataset. In *2017 IEEE Conference on Computer Vision and Pattern Recognition (CVPR)*, pages 4724–4733, July 2017. doi: 10.1109/CVPR.2017.502.
- [5] Mengyuan Chen, Junyu Gao, Shicai Yang, and Changsheng Xu. Dual-Evidential Learning for Weakly-supervised Temporal Action Localization. In Shai Avidan, Gabriel Brostow, Moustapha Cissé, Giovanni Maria Farinella, and Tal Hassner, editors, *Computer Vision – ECCV 2022*, Lecture Notes in Computer Science, pages 192–208, Cham, 2022. Springer Nature Switzerland. ISBN 978-3-031-19772-7. doi: 10.1007/978-3-031-19772-7\_12.
- [6] Anthony Cioppa, Adrien Deliege, Silvio Giancola, Bernard Ghanem, Marc Van Droogenbroeck, Rikke Gade, and Thomas B. Moeslund. A Context-Aware Loss Function for Action Spotting in Soccer Videos. In *2020 IEEE/CVF Conference on Computer Vision and Pattern Recognition (CVPR)*, pages 13123–13133, Seattle, WA, USA, June 2020. IEEE. ISBN 978-1-72817-168-5. doi: 10.1109/CVPR42600.2020.01314.
- [7] Dima Damen, Teesid Leelasawassuk, Osian Haines, Andrew Calway, and W. Mayol-Cuevas. You-Do, I-Learn: Discovering Task Relevant Objects and their Modes of Interaction from Multi-User Ego-centric Video. In *British Machine Vision Conference (BMVC)*, Nottingham, UK, 2014.
- [8] A. Dutta, A. Gupta, and A. Zissermann. VGG Image Annotator (VIA), 2016.
- [9] Abhishek Dutta and Andrew Zisserman. The VIA Annotation Software for Images, Audio and Video. In *Proceedings of the 27th ACM International Conference on Multimedia*, MM '19, New York, NY,

- USA, 2019. ACM. ISBN 978-1-4503-6889-6. doi: 10.1145/3343031.3350535.
- [10] Alireza Fathi, Xiaofeng Ren, and James M. Rehg. Learning to recognize objects in egocentric activities. In *CVPR 2011*, pages 3281–3288, June 2011. doi: 10.1109/CVPR.2011.5995444.
- [11] R. A. Fisher. The arrangement of field experiments. *Journal of the Ministry of Agriculture*, 33:503–515, 1926. ISSN 0368-3087. doi: 10.23637/rothamsted.8v61q.
- [12] Silvio Giancola, Mohieddine Amine, Tarek Dghaily, and Bernard Ghanem. SoccerNet: A Scalable Dataset for Action Spotting in Soccer Videos. In *2018 IEEE/CVF Conference on Computer Vision and Pattern Recognition Workshops (CVPRW)*, pages 1792–179210, Salt Lake City, UT, June 2018. IEEE. ISBN 978-1-5386-6100-0. doi: 10.1109/CVPRW.2018.00223.
- [13] Fabian Caba Heilbron, Victor Escorcia, Bernard Ghanem, and Juan Carlos Niebles. ActivityNet: A large-scale video benchmark for human activity understanding. In *Proceedings of the IEEE Conference on Computer Vision and Pattern Recognition*, pages 961–970, 2015.
- [14] Linjiang Huang, Yan Huang, Wanli Ouyang, and Liang Wang. Relational Prototypical Network for Weakly Supervised Temporal Action Localization. *Proceedings of the AAAI Conference on Artificial Intelligence*, 34(07):11053–11060, April 2020. ISSN 2374-3468. doi: 10.1609/aaai.v34i07.6760.
- [15] Linjiang Huang, Liang Wang, and Hongsheng Li. Weakly Supervised Temporal Action Localization via Representative Snippet Knowledge Propagation. In *2022 IEEE/CVF Conference on Computer Vision and Pattern Recognition (CVPR)*, pages 3262–3271, June 2022. doi: 10.1109/CVPR52688.2022.00327.
- [16] Y.-G. Jiang, J. Liu, A. Roshan Zamir, G. Toderici, I. Laptev, M. Shah, and R. Sukthankar. THUMOS Challenge: Action Recognition with a Large Number of Classes, 2014.
- [17] Chen Ju, Peisen Zhao, Siheng Chen, Ya Zhang, Yanfeng Wang, and Qi Tian. Divide and Conquer for Single-frame Temporal Action Localization. In *2021 IEEE/CVF International Conference on Computer Vision (ICCV)*, pages 13435–13444, October 2021. doi: 10.1109/ICCV48922.2021.01320.
- [18] Prannay Khosla, Piotr Teterwak, Chen Wang, Aaron Sarna, Yonglong Tian, Phillip Isola, Aaron Maschinot, Ce Liu, and Dilip Krishnan. Supervised Contrastive Learning. In *Advances in Neural Information Processing Systems*, volume 33, pages 18661–18673. Curran Associates, Inc., 2020.
- [19] Pilhyeon Lee and Hyeran Byun. Learning Action Completeness From Points for Weakly-Supervised Temporal Action Localization. In *Proceedings of the IEEE/CVF International Conference on Computer Vision (ICCV)*, pages 13648–13657, October 2021.
- [20] Pilhyeon Lee, Youngjung Uh, and Hyeran Byun. Background Suppression Network for Weakly-Supervised Temporal Action Localization. *Proceedings of the AAAI Conference on Artificial Intelligence*, 34(07):11320–11327, April 2020. ISSN 2374-3468. doi: 10.1609/aaai.v34i07.6793.
- [21] Pilhyeon Lee, Jinglu Wang, Yan Lu, and Hyeran Byun. Weakly-supervised Temporal Action Localization by Uncertainty Modeling. *Proceedings of the AAAI Conference on Artificial Intelligence*, 35(3):1854–1862, May 2021. ISSN 2374-3468. doi: 10.1609/aaai.v35i3.16280.
- [22] Ping Li, Jiachen Cao, and Xingchao Ye. Prototype contrastive learning for point-supervised temporal action detection. *Expert Systems with Applications*, 213:118965, March 2023. ISSN 0957-4174. doi: 10.1016/j.eswa.2022.118965.
- [23] Ronglu Li, Tianyi Zhang, and Rubo Zhang. Weakly supervised temporal action localization: A survey. *Multimedia Tools and Applications*, pages 1–26, February 2024. ISSN 1573-7721. doi: 10.1007/s11042-024-18554-9.
- [24] Zhe Li, Yazan Abu Farha, and Jurgen Gall. Temporal Action Segmentation From Timestamp Supervision. In *Proceedings of the IEEE/CVF Conference on Computer Vision and Pattern Recognition*, pages 8365–8374, 2021. doi: 10.1109/CVPR46437.2021.00826.
- [25] Zhi Li, Lu He, and Huijuan Xu. Weakly-Supervised Temporal Action Detection for Fine-Grained Videos with Hierarchical Atomic Actions. In Shai Avidan, Gabriel Brostow, Moustapha Cissé, Giovanni Maria Farinella, and Tal Hassner, editors, *Computer Vision – ECCV 2022*, pages 567–584, Cham, 2022. Springer Nature Switzerland. ISBN 978-3-031-20080-9. doi: 10.1007/978-3-031-20080-9\_33.
- [26] Tianwei Lin, Xiao Liu, Xin Li, Errui Ding, and Shilei Wen. BMN: Boundary-Matching Network for Temporal Action Proposal Generation. In *2019 IEEE/CVF International Conference on Computer Vision (ICCV)*, pages 3888–3897. IEEE Computer Society, October 2019. ISBN 978-1-72814-803-8. doi: 10.1109/ICCV.2019.00399.
- [27] Tsung-Yi Lin, Priya Goyal, Ross Girshick, Kaiming He, and Piotr Dollár. Focal Loss for Dense Object Detection. *IEEE Transactions on Pattern Analysis and Machine Intelligence*, 42(2):318–327, February 2020. ISSN 1939-3539. doi: 10.1109/TPAMI.2018.2858826.
- [28] Daochang Liu, Tingting Jiang, and Yizhou Wang. Completeness Modeling and Context Separation for Weakly Supervised Temporal Action Localization.

- In *2019 IEEE/CVF Conference on Computer Vision and Pattern Recognition (CVPR)*, pages 1298–1307, June 2019. doi: 10.1109/CVPR.2019.00139.
- [29] Qinying Liu, Zilei Wang, Shenghai Rong, Junjie Li, and Yixin Zhang. Revisiting Foreground and Background Separation in Weakly-supervised Temporal Action Localization: A Clustering-based Approach. In *Proceedings of the IEEE/CVF International Conference on Computer Vision*, pages 10433–10443, 2023. doi: 10.1109/ICCV51070.2023.00957.
- [30] Yi Liu, Limin Wang, Yali Wang, Xiao Ma, and Yu Qiao. FineAction: A fine-grained video dataset for temporal action localization. *IEEE Transactions on Image Processing*, 31:6937–6950, 2022. doi: 10.1109/TIP.2022.3217368.
- [31] Fan Ma, Linchao Zhu, Yi Yang, Shengxin Zha, Gourab Kundu, Matt Feiszli, and Zheng Shou. SF-Net: Single-Frame Supervision for Temporal Action Localization. In Andrea Vedaldi, Horst Bischof, Thomas Brox, and Jan-Michael Frahm, editors, *Computer Vision – ECCV 2020*, Lecture Notes in Computer Science, pages 420–437, Cham, 2020. Springer International Publishing. ISBN 978-3-030-58548-8. doi: 10.1007/978-3-030-58548-8\_25.
- [32] Junwei Ma, Satya Krishna Gorti, Maksims Volkovs, and Guangwei Yu. Weakly Supervised Action Selection Learning in Video. In *Proceedings of the IEEE/CVF Conference on Computer Vision and Pattern Recognition*, pages 7587–7596, 2021. doi: 10.1109/CVPR46437.2021.00750.
- [33] Kyle Min and Jason J. Corso. Adversarial Background-Aware Loss for Weakly-Supervised Temporal Activity Localization. In Andrea Vedaldi, Horst Bischof, Thomas Brox, and Jan-Michael Frahm, editors, *Computer Vision – ECCV 2020*, Lecture Notes in Computer Science, pages 283–299, Cham, 2020. Springer International Publishing. ISBN 978-3-030-58568-6. doi: 10.1007/978-3-030-58568-6\_17.
- [34] Davide Moltisanti, Sanja Fidler, and Dima Damen. Action Recognition From Single Timestamp Supervision in Untrimmed Videos. In *2019 IEEE/CVF Conference on Computer Vision and Pattern Recognition (CVPR)*, pages 9907–9916. IEEE Computer Society, June 2019. ISBN 978-1-72813-293-8. doi: 10.1109/CVPR.2019.01015.
- [35] Sanath Narayan, Hisham Cholakkal, Munawar Hayat, Fahad Shahbaz Khan, Ming-Hsuan Yang, and Ling Shao. D2-Net: Weakly-Supervised Action Localization via Discriminative Embeddings and Denoised Activations. In *2021 IEEE/CVF International Conference on Computer Vision (ICCV)*, pages 13588–13597, October 2021. doi: 10.1109/ICCV48922.2021.01335.
- [36] Phuc Nguyen, Bohyung Han, Ting Liu, and Gautam Prasad. Weakly Supervised Action Localization by Sparse Temporal Pooling Network. In *2018 IEEE/CVF Conference on Computer Vision and Pattern Recognition*, pages 6752–6761, Salt Lake City, UT, USA, June 2018. IEEE. ISBN 978-1-5386-6420-9. doi: 10.1109/CVPR.2018.00706.
- [37] Sujoy Paul, Sourya Roy, and Amit K. Roy-Chowdhury. W-TALC: Weakly-Supervised Temporal Activity Localization and Classification. In Vittorio Ferrari, Martial Hebert, Cristian Sminchisescu, and Yair Weiss, editors, *Computer Vision – ECCV 2018*, Lecture Notes in Computer Science, pages 588–607, Cham, 2018. Springer International Publishing. ISBN 978-3-030-01225-0. doi: 10.1007/978-3-030-01225-0\_35.
- [38] Sanqing Qu, Guang Chen, Zhijun Li, Lijun Zhang, Fan Lu, and Alois Knoll. ACM-Net: Action Context Modeling Network for Weakly-Supervised Temporal Action Localization, April 2021.
- [39] Zheng Shou, Hang Gao, Lei Zhang, Kazuyuki Miyazawa, and Shih-Fu Chang. AutoLoc: Weakly-Supervised Temporal Action Localization in Untrimmed Videos. In Vittorio Ferrari, Martial Hebert, Cristian Sminchisescu, and Yair Weiss, editors, *Computer Vision – ECCV 2018*, Lecture Notes in Computer Science, pages 162–179, Cham, 2018. Springer International Publishing. ISBN 978-3-030-01270-0. doi: 10.1007/978-3-030-01270-0\_10.
- [40] Krishna Kumar Singh and Yong Jae Lee. Hide-and-Seek: Forcing a Network to be Meticulous for Weakly-Supervised Object and Action Localization. In *2017 IEEE International Conference on Computer Vision (ICCV)*, pages 3544–3553, October 2017. doi: 10.1109/ICCV.2017.381.
- [41] Waqas Sultani, Chen Chen, and Mubarak Shah. Real-World Anomaly Detection in Surveillance Videos. In *2018 IEEE/CVF Conference on Computer Vision and Pattern Recognition*, pages 6479–6488, Salt Lake City, UT, June 2018. IEEE. ISBN 978-1-5386-6420-9. doi: 10.1109/CVPR.2018.00678.
- [42] Chen Sun, Sanketh Shetty, Rahul Sukthankar, and Ram Nevatia. Temporal Localization of Fine-Grained Actions in Videos by Domain Transfer from Web Images. In *Proceedings of the 23rd ACM International Conference on Multimedia*, MM ’15, pages 371–380, New York, NY, USA, October 2015. Association for Computing Machinery. ISBN 978-1-4503-3459-4. doi: 10.1145/2733373.2806226.
- [43] Christian Szegedy, Wei Liu, Yangqing Jia, Pierre Sermanet, Scott Reed, Dragomir Anguelov, Dumitru Erhan, Vincent Vanhoucke, and Andrew Rabinovich. Going Deeper with Convolutions, September 2014.
- [44] Elahe Vahdani and Yingli Tian. Deep Learning-based Action Detection in Untrimmed Videos: A Survey. *IEEE Transactions on Pattern Analysis and*

*Machine Intelligence*, pages 1–20, 2022. ISSN 0162-8828, 2160-9292, 1939-3539. doi: 10.1109/TPAMI.2022.3193611.

- [45] Sarvesh Vishwakarma and Anupam Agrawal. A survey on activity recognition and behavior understanding in video surveillance. *The Visual Computer*, 29(10):983–1009, October 2013. ISSN 1432-2315. doi: 10.1007/s00371-012-0752-6.
- [46] Guiqin Wang, Peng Zhao, Cong Zhao, Shusen Yang, Jie Cheng, Luziwei Leng, Jianxing Liao, and Qinghai Guo. Weakly-Supervised Action Localization by Hierarchically-Structured Latent Attention Modeling. In *Proceedings of the IEEE/CVF International Conference on Computer Vision*, pages 10203–10213, 2023. doi: 10.1109/ICCV51070.2023.00936.
- [47] Limin Wang, Yuanjun Xiong, Dahua Lin, and Luc Van Gool. UntrimmedNets for Weakly Supervised Action Recognition and Detection. In *2017 IEEE Conference on Computer Vision and Pattern Recognition (CVPR)*, pages 6402–6411. IEEE Computer Society, July 2017. ISBN 978-1-5386-0457-1. doi: 10.1109/CVPR.2017.678.
- [48] Huifen Xia and Yongzhao Zhan. A Survey on Temporal Action Localization. *IEEE Access*, 8:70477–70487, 2020. ISSN 2169-3536. doi: 10.1109/ACCESS.2020.2986861.
- [49] Mengmeng Xu, Chen Zhao, David S. Rojas, Ali Thabet, and Bernard Ghanem. G-TAD: Sub-Graph Localization for Temporal Action Detection. In *2020 IEEE/CVF Conference on Computer Vision and Pattern Recognition (CVPR)*, pages 10153–10162, Seattle, WA, USA, June 2020. IEEE. ISBN 978-1-72817-168-5. doi: 10.1109/CVPR42600.2020.01017.
- [50] Chen-Lin Zhang, Jianxin Wu, and Yin Li. ActionFormer: Localizing Moments of Actions with Transformers. In Shai Avidan, Gabriel Brostow, Moustapha Cissé, Giovanni Maria Farinella, and Tal Hassner, editors, *Computer Vision – ECCV 2022*, Lecture Notes in Computer Science, pages 492–510, Cham, 2022. Springer Nature Switzerland. ISBN 978-3-031-19772-7. doi: 10.1007/978-3-031-19772-7\_29.